Imaging nanoscale features with plasmon-coupled leakage radiation far-field superlenses

Charles J. Regan,[1,2] Robier Rodriguez,[3] Shivkumar C. Gourshetty,[1,2] Luis Grave de Peralta,[2,3] and Ayrton A. Bernussi[1,2,*]

[1]*Department of Electrical and Computer Engineering, Texas Tech University, Lubbock, TX 79409, USA*
[2]*Nano Tech Center, Texas Tech University, Lubbock, TX 79409, USA*
[3]*Department of Physics, Texas Tech University, Lubbock, TX 79409, USA*
[*]*ayrton.bernussi@ttu.edu*

Abstract: Optical images from nano-scale features were obtained by collection of leakage radiation coupled to surface plasmon polaritons excited by near-field fluorescence. Plasmonic crystals with spatial periods as small as 190 nm and non-periodic features separated by 80 nm, corresponding to ~λ/7, were clearly visible in the real plane images using this far-field technique. We show that the leaked light from the investigated samples carries detailed information to the far-field which is not present in the images obtained with conventional optical microscopy.

OCIS codes: (110.0180) Microscopy; (240.6680) Surface plasmons.

References and links

1. J. B. Pendry, "Negative refraction makes a perfect lens," Phys. Rev. Lett. **85**(18), 3966–3969 (2000).
2. D. O. S. Melville and R. J. Blaikie, "Super-resolution imaging through a planar silver layer," Opt. Express **13**(6), 2127–2134 (2005).
3. Z. Liu, S. Durant, H. Lee, Y. Pikus, N. Fang, Y. Xiong, C. Sun, and X. Zhang, "Far-field optical superlens," Nano Lett. **7**(2), 403–408 (2007).
4. Z. Liu, H. Lee, Y. Xiong, C. Sun, and X. Zhang, "Far-field optical hyperlens magnifying sub-diffraction-limited objects," Science **315**(5819), 1686 (2007).
5. S. Durant, Z. Liu, J. M. Steele, and X. Zhang, "Theory of the transmission properties of an optical far-field superlens for imaging beyond the diffraction limit," J. Opt. Soc. Am. B **23**(11), 2383–2392 (2006).
6. Z. Jacob, L. V. Alekseyev, and E. Narimanov, "Optical hyperlens: far-field imaging beyond the diffraction limit," Opt. Express **14**(18), 8247–8256 (2006).
7. A. V. Kildishev and E. E. Narimanov, "Impedance-matched hyperlens," Opt. Lett. **32**(23), 3432–3434 (2007).
8. H. Lee, Z. Liu, Y. Xiong, C. Sun, and X. Zhang, "Development of optical hyperlens for imaging below the diffraction limit," Opt. Express **15**(24), 15886–15891 (2007).
9. Y. Xiong, Z. Liu, C. Sun, and X. Zhang, "Two-dimensional imaging by far-field superlens at visible wavelengths," Nano Lett. **7**(11), 3360–3365 (2007).
10. Y. Xiong, Z. Liu, S. Durant, H. Lee, C. Sun, and X. Zhang, "Tuning the far-field superlens: from UV to visible," Opt. Express **15**(12), 7095–7102 (2007).
11. I. I. Smolyaninov, Y. J. Hung, and C. C. Davis, "Magnifying superlens in the visible frequency range," Science **315**(5819), 1699–1701 (2007).
12. S. P. Frisbie, C. F. Chesnutt, M. E. Holtz, A. Krishnan, L. de Peralta, and A. A. Bernussi, "Image formation in wide-field microscopes based on leakage of surface plasmon-coupled fluorescence," IEEE Photon. J. **1**(2), 153–162 (2009).
13. C. J. Regan, O. Thiabgoh, L. Grave de Peralta, and A. A. Bernussi, "Probing photonic Bloch wavefunctions with plasmon-coupled leakage radiation," Opt. Express **20**(8), 8658–8666 (2012).
14. H. Raether, *Surface Plasmons on Smooth and Rough Surfaces and Gratings* (Springer-Verlag, 1988).
15. J. R. Lakowicz, "Radiative decay engineering 3. Surface plasmon-coupled directional emission," Anal. Biochem. **324**(2), 153–169 (2004).
16. I. Gryczynski, J. Malicka, Z. Gryczynski, and J. R. Lakowicz, "Surface plasmon-coupled emission with gold films," J. Phys. Chem. B **108**(33), 12568–12574 (2004).
17. A. Giannattasio and W. L. Barnes, "Direct observation of surface plasmon-polariton dispersion," Opt. Express **13**(2), 428–434 (2005).
18. C. J. Regan, A. Krishnan, R. Lopez-Boada, L. Grave de Peralta, and A. A. Bernussi, "Direct observation of photonic Fermi surfaces by plasmon tomography," Appl. Phys. Lett. **98**(15), 151113 (2011).
19. P. Chaturvedi, W. Wu, V. J. Logeeswaran, Z. Yu, M. S. Islam, S. Y. Wang, R. Williams, and N. X. Fang, "A smooth optical superlens," Appl. Phys. Lett. **96**(4), 043102 (2010).

#171631 - $15.00 USD Received 3 Jul 2012; revised 1 Aug 2012; accepted 22 Aug 2012; published 28 Aug 2012

1. Introduction

Conventional optical microscopy is diffraction-limited to spatial periods larger than λ/NA, where λ is the free space wavelength of the illuminating light, and NA is the numerical aperture of the system [1,2]. In the last few years considerable efforts have been dedicated to overcoming this fundamental limit. For instance, Pendry proposed that a thin metal film could be used to image features beyond the diffraction limit in the near-field [1]. This was later confirmed experimentally [2]. The proposed superlens approach relies on the principle that the diffraction limit is reached when sufficiently small features diffract some of the incident energy into evanescent waves. Pendry showed that a thin metal layer can be used to enhance the evanescent field and therefore sub-diffraction limited features can be imaged in the near-field. Far-field superlenses, also based on the enhancement of the evanescent field by metal layers have been investigated both theoretically and experimentally [3–11]. More recently, Liu *et al.* demonstrated a far-field superlens which incorporates patterned periodic metallic features that converts evanescent waves into propagating waves [3]. Although sub-diffraction limited features can be imaged with this method, it requires multiple fabrication steps and the utilization of a linear grating to frustrate the evanescent waves. Also, this type of superlens is narrowband due to the resonant out-coupling condition of the grating, and does not produce a direct image of the investigated features. It requires numerical reconstruction to obtain the images. Therefore, alternative approaches to optically image sub-diffraction limited features in the *far-field* are of particular importance.

In this work, we report new experimental results concerning images of sub-diffraction limited features in the far-field using a superlens with a non-patterned metallic layer. Our approach relies on the imaging of surface plasmon polaritons (SPP) coupled to leakage radiation excited by near-field fluorescence, or plasmon coupled leakage radiation (PCLR) for short [12]. Major advantages of using fluorescent coupled SPP excitation include: large coupling efficiency between the excited fluorophores and SPPs; SPP propagation occurs in all allowed directions on the sample surface; and most of the light that is not SPP-coupled (direct laser excitation and light diffraction from the features in the sample) can be practically eliminated with the aid of narrow-band interference filters. The combination of these attributes results in superior image clarity and definition when compared to other approaches. The sub-diffraction imaging capabilities of the PCLR technique is a direct result of the SPP propagation within the sample, which is modified by *in-plane* scattering perturbations by the dielectric features, as previously shown for the specific case of Bloch functions in periodic plasmonic structures [13]. This is in contrast to the out-of-plane diffraction effects which comprises the basis for image formation in conventional optical microscopy. We stress here that the reason why the PCLR technique is not diffraction limited is precisely because the light collected to form the images is not related by out-of-plane diffraction by the surface features. Rather, the light coupled to the SPPs in the samples occurs in all directions and are in-plane scattered by the surface features. This adds further information to the electric field of the propagating in-plane SPPs in the sample. Then the propagating SPPs leak continuously to the substrate where they can be collected and imaged. The resolution limit and image definition of the PCLR technique is determined by the in-plane diffraction of the SPPs by the features in the sample surface, and on the scattering strength of these individual features. This implies that the ultimate ability to resolve individual features is reliant on their ability to modify the in-plane electric field, which manifests in contrast changes in the final image. Furthermore, the PCLR technique allows for imaging nano-size features in the far-field without the need of complex superlens structure designs or sample post-processing [3]. Importantly, this makes the PCLR-superlens technique rather broadband (to the extent that the metal in use can support SPPs with relatively low loss), whereas the previously proposed periodic lens structure is inherently narrowband due to the out-coupling grating patterned into the metal lens [3]. Another significant advantage of the PCLR-superlens approach is its ability to obtain super-resolution images directly in the real plane or surface image (SE) as

#171631 - $15.00 USD Received 3 Jul 2012; revised 1 Aug 2012; accepted 22 Aug 2012; published 28 Aug 2012

opposed to having to be reconstructed numerically [3]. This important attribute can be used in future projection nanolithography applications.

2. Theory of plasmon-coupled leakage imaging

In order to analyze the sub-diffraction characteristics of the PCLR-superlens approach we investigated two different nano-structures: a dielectric-loaded plasmonic crystal (Fig. 1(a)) and a chromium double-line (Fig. 1(b)). Firstly we consider the plasmonic crystal which comprises a periodic array of dye-doped dielectric features defined on the top of a gold thin film, which is in turn above a glass substrate (see Fig. 1(a)).

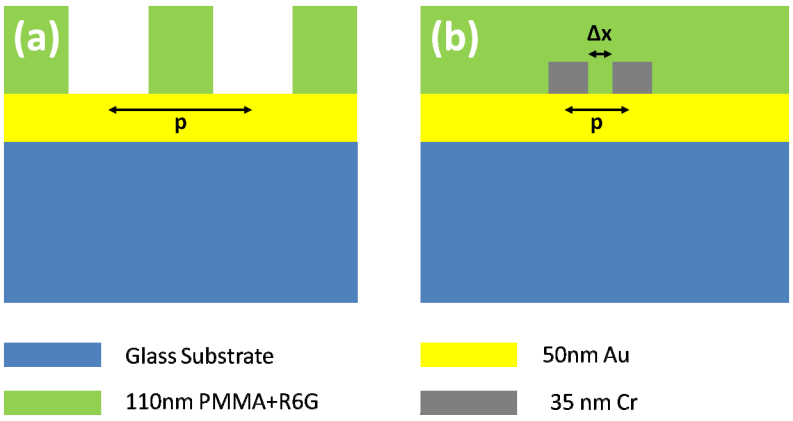

Fig. 1. Schematic illustrations of (a) dye-doped dielectric-loaded plasmonic crystal and (b) nano-sized Cr double lines.

In our studies we used samples comprising ~150 μm glass substrates covered with a 50 nm thick gold layer and coated with a ~110 nm thick doped PMMA layer. The real part of the effective refractive index of the allowed propagating SPP mode was calculated, using Finite Element Analysis (COMSOL Multiphysics®), as $n_{eff} = 1.03$. This value is less than that of the substrate, and thus the SPPs will couple (or "leak") to the substrate with a given SPP resonance angle (θ_{SPR}) [14]. For a uniform (non-patterned) dye-doped dielectric layer over the gold film, the θ_{SPR} angle is determined by the momentum matching condition:

$$k_{spp} = k_o n_{eff} = k_o n_{sub} \sin(\theta_{SPR}) \quad (1)$$

where k_{spp} is the wavevector of the SPP, k_0 is the freespace wavevector, n_{eff} is the effective refractive index of the propagating mode, and n_{sub} is the substrate refractive index. When light is coupled to the SPPs, via fluorescent excitation, it propagates in all directions in the sample surface and then leaks into the glass substrate [15,16].The leakage radiation is then collected and imaged into the Fourier Plane (FP) with a signature corresponding to a single ring [15,16]. When the SPPs propagate in a periodic patterned surface, k_{spp} is modified by $G = 2\pi/p$, which corresponds to the reciprocal lattice vector of the crystal, where p is the period of the lattice in the real space. In this case, the momentum matching condition is given by:

$$k_o n_{eff} \pm G = k_o n_{sub} \sin(\theta_{SPR}) \quad (2)$$

The corresponding FP images of plasmonic crystals now involve multiple rings displaced from each other by the vector G (see Fig. 2(a)) [17].

#171631 - $15.00 USD Received 3 Jul 2012; revised 1 Aug 2012; accepted 22 Aug 2012; published 28 Aug 2012

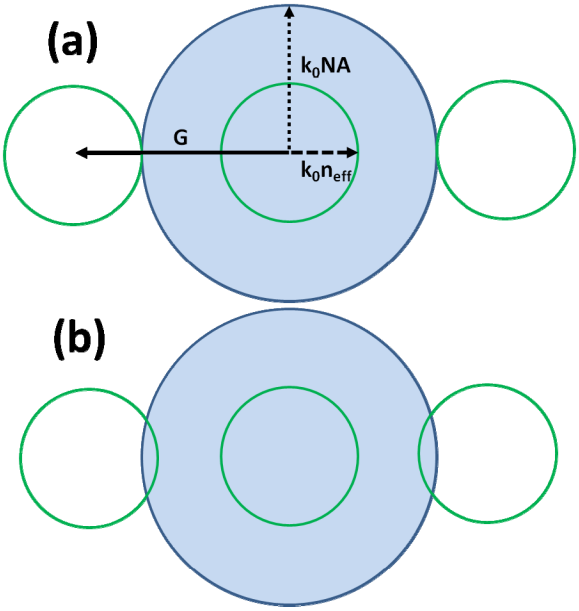

Fig. 2. Schematics of FP images obtained with the PCLR-superlens technique. (a) when the spatial period is just at the limit of resolvability, and (b) when the features will be resolvable.

These multiple rings carry detailed information about the periodic structure in the BFP image of plasmonic structures using the PCLR technique, just as the diffraction spots do in conventional optical microscopy. To be imaged, this implies that the light must leak with an angle smaller than the maximum angle collected by the collecting microscope objective, determined by its numerical aperture (NA) (See Fig. 2(b)). This gives:

$$\left|\vec{k}_o n_{eff} \pm \vec{G}\right| < \left|\vec{k}_o NA\right| \tag{3}$$

From Eq. (3) we can determine the minimum period resolvable in a periodic structure using the PCLR technique as:

$$p > \frac{\lambda}{NA + n_{eff}} \tag{4}$$

with the constraint that n_{eff} must be less than the substrate refractive index in order to ensure leakage collection by the imaging system. This is a key result since it shows a marked difference in resolving power from diffraction-limited optical systems. An estimate of the resolution limit of the PCLR technique for non-periodic structures can be obtained considering that the minimum period corresponds to a maximum resolvable wavevector $k_{max} = k_o(NA + n_{eff})$ with an angular bandwidth of $\Delta k = 2k_{max}$. Therefore, using $\Delta k \Delta x \approx 2\pi$, the expected single-feature resolution can be determined as:

$$\Delta x \approx \frac{\lambda}{2\left(NA + n_{eff}\right)} \tag{5}$$

For instance, if $n_{eff} \sim NA = 1.49$ and $\lambda = 568$ nm, the resolution limit of the superlens-PCLR technique would be $p > \lambda/2NA = 190$ nm and $\Delta x \approx \lambda/6$, which are already well-below the classical optical diffraction limit which is estimated as $p > \lambda/NA = 381$ nm and $\Delta x \approx \lambda/2NA \approx \lambda/3$.

#171631 - $15.00 USD Received 3 Jul 2012; revised 1 Aug 2012; accepted 22 Aug 2012; published 28 Aug 2012

3. Experimental confirmation of resolution

We confirmed the sub-diffraction imaging capabilities of the superlens-PCLR technique [12] by fabricating dielectric-loaded plasmonic crystals consisting of 110 nm thick PMMA doped with Rhodamine-6G (R6G), which was spun on the top of 50 nm thick gold films deposited on glass substrates. Arrays of holes arranged in square lattice crystal symmetry were defined on the dye-doped PMMA using a combination of electron-beam lithography and lift-off techniques. FP and SE images were obtained by illuminating the patterned side of the samples with a continuous-wave laser emitting at 532 nm wavelength. The fluorescent emission, centered at ~568 nm wavelength, couples to the SPPs in the sample and their propagation directions are modified, from the un-patterned layer, by the presence of the periodic structure [18]. The leaked light with the SPR angle, defined in Eq. (3), is collected by a microscope objective with NA = 1.49, band-pass filtered at 568 nm wavelength, and then imaged on both the real and Fourier planes, using a commercial inverted microscope [12,18]. A schematic illustration of the experimental PCLR setup is depicted in Fig. 3.

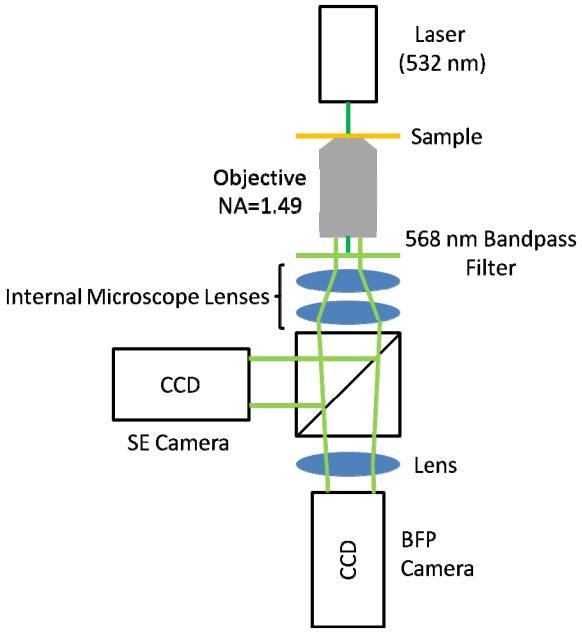

Fig. 3. Schematic illustration of the PCLR-superlens imaging setup.

We fabricated several plasmonic crystals with different lattice periods to verify experimentally the condition defined in Eq. (4), which corresponds to a critical lattice period where the holes are no longer visible in the SE images of these structures. For the samples analyzed here with PMMA and gold thicknesses of ~110 nm and 50 nm, respectively, corresponding to n_{eff} = 1.03, we anticipate a resolution limit near p = 225nm, well below of the classical optical diffraction limit p = 381 nm. In our plasmonic crystal samples we used holes with radius $p/3$, and this corresponds to edge-to-edge separation between holes of 75 nm. Figure 4 shows SE and FP images of plasmonic crystals with three different periods.

#171631 - $15.00 USD Received 3 Jul 2012; revised 1 Aug 2012; accepted 22 Aug 2012; published 28 Aug 2012

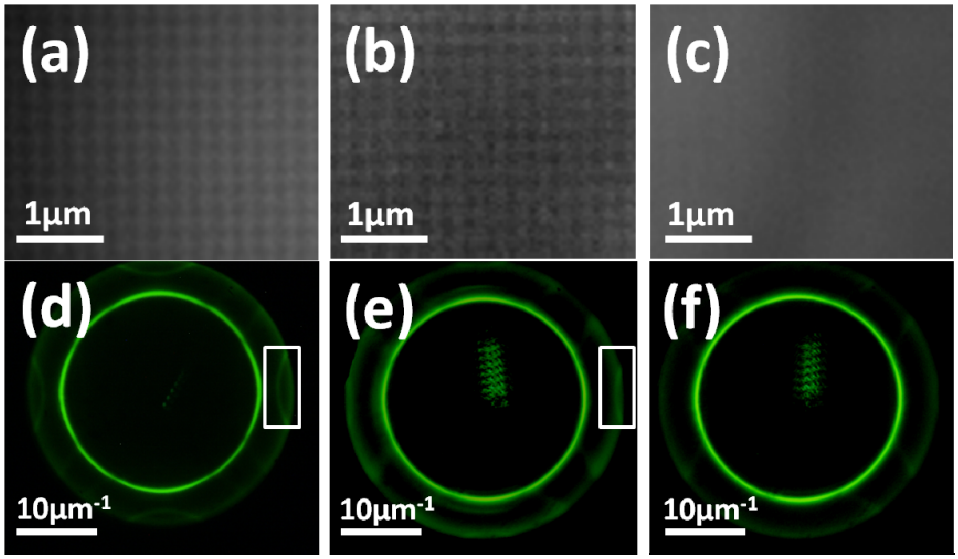

Fig. 4. SE images of dye doped dielectric loaded plasmonic crystals with periods 240 nm (a), 235 nm (b),and 230 nm (c). Corresponding FP images are shown in (d), (e), (f), respectively. For (a) and (b) the crystal features are resolvable, which is evident in (d) and (e) by the first order extra rings present (encircled in white boxes).

The SE image resolves individual holes for lattice periods p = 240 nm (Fig. 4(a)) and p = 235 nm (Fig. 4(b)), but for p = 230 nm the image shows a uniform surface. Figures 4(d)-4(f) shows the corresponding FP images to the same samples shown in Figs. 4(a)-4(c). The characteristic first order extra rings (marked by a white box) can be only observed in the FP images shown Figs. 4(d) and 4(e), where holes in the surface of the sample were also visible (Figs. 4(a) and 4(b)). However, the absence of first order extra rings in the FP of the plasmonic crystal (Fig. 4(f)) and the corresponding uniform surface shown in Fig. 4(c) confirms that p = 230 nm is the minimum period resolvable in the investigated plasmonic structures. The small discrepancy between measured (p = 230nm) and calculated (p = 225nm) minimum period is attributed to deviations (of the order of few nanometers) in the hole diameter and period from their nominal values and imprecision in the determination of the effective refractive index of the plasmon guided mode. These findings, confirm the super-resolution capability of the far-field PCLR approach for periodic features.

4. Non-periodic far-field super-resolution

To further explore the imaging capabilities of the PCLR-superlens technique, and to show that individual features with sub-diffraction dimensions can be also imaged, in addition to periodic structures, we fabricated a second type of sample as shown in Fig. 1(b). The samples comprise two parallel lines (120 nm wide each and 50 μm long) of chromium (~35 nm thick) patterned on the top of the uniform gold layer (50 nm thick), with edge-to-edge line separation (Δx) of 80 nm. The whole sample was then covered with 110 nm thick R6G-PMMA. We performed a direct comparison among Scanning Electron Microscopy (SEM), SE, and white light (WL) images of the fabricated double-lines. The WL images were obtained using conventional microscopy under white light illumination, but filtering at 568 nm wavelength, in order to keep the same conditions between experiments. The PCLR technique was also used to obtain SE images of the fabricated structures. In contrast to the plasmonic crystals, where the SPP propagation is determined by the patterned holes in the PMMA, the chromium metal layer now modifies the propagating SPPs in the double line samples. Figure 5 shows representative SEM (Fig. 5(a)), SE (Fig. 5(b)), and WL (Fig. 5(c)) images of a Cr/Au double-line sample.

#171631 - $15.00 USD Received 3 Jul 2012; revised 1 Aug 2012; accepted 22 Aug 2012; published 28 Aug 2012

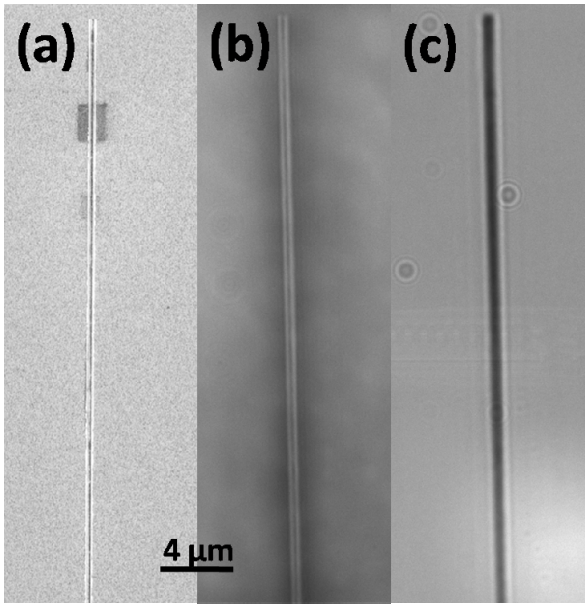

Fig. 5. SEM (a), PCLR (b), and WL (c) images of 35 nm thick and 120 nm wide Cr double lines defined on the top of the gold layer. The double-line center-to-center (*p)* separation is 200 nm with an 80 nm gap between the lines.

The SEM image was obtained at approximately the same magnification as the optical images. The SE image (Fig. 5(b)) clearly shows the presence of the two patterned chromium lines with dimensions comparable to that obtained by the SEM image (Fig. 5(a)) from the same sample. In contrast, the WL image (Fig. 5(c)) shows that the double lines cannot be resolved under white light illumination. In order to further explore this effect, we zoom in (by a factor of ~10) the SEM, SE, and WL images shown in Fig. 5, and the corresponding magnified images are shown in Figs. 6(a), 6(b), and 6(c), respectively. Again, the WL image (Fig. 6(c)) clearly does not resolve the double lines while the SE image (Fig. 6(b)) shows the double lines with an intensity contrast 3:1. This can be further confirmed in Fig. 6(d) where we plot the intensity profiles of the images shown in Figs. 6(b) and 6(c). In the case of the SE image (Fig. 6(b)) the line profile reveals two well-defined peaks. In contrast, the line profile corresponding to the WL image (Fig. 6(c)) shows a broad single band with no resolvable features. These findings, confirm the super-resolution capability of the far-field PCLR approach for non-periodic features.

In the SE images shown in Figs. 5(b) and 6(b), the definition of the two chromium lines, which has 80 nm gap between the edges of the lines, is close to the resolution limit of our current PCLR setup. However, additional limiting resolution factors, extrinsic to the PCLR technique, may be playing an important role in determining the maximum resolvable features that can be obtained from these particular experiments. Two important factors are of significance: the gold grain size (~50 nm in lateral size) and the magnification and camera resolution limitations of our microscope. Further imaging resolution improvements can be achieved in the PCLR system by using less granular gold films, for example with the aid of germanium wetting layer [19], in combination with higher image resolution cameras. Another possible alternative to further improve the resolution limit of the PCLR technique is to use non-dye doped coated samples under direct excitation with shorter illumination wavelengths. However, it should be pointed out here that the anticipated image quality using that approach is expected to be inferior to the images shown in this work due to reduced SPP coupling excitation efficiency, non-uniform SPP excitation, SPP propagation is limited to specific directions within the sample, and the need of a spatial filter to block the incident laser beam in the Fourier plane.

#171631 - $15.00 USD Received 3 Jul 2012; revised 1 Aug 2012; accepted 22 Aug 2012; published 28 Aug 2012

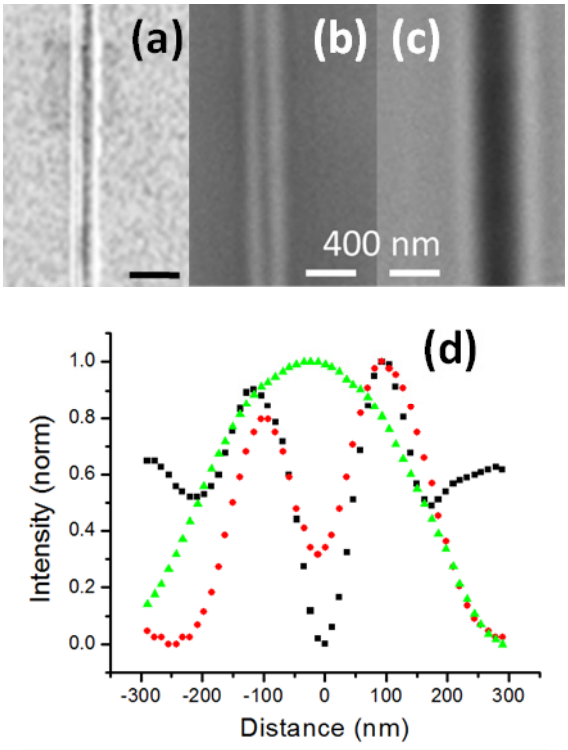

Fig. 6. Expanded view of the images shown in Fig. 5(a), Fig. 5(b) and Fig. 5(c). (a) SEM image, (b) PCLR image and (c) WL image. (d) line intensity profiles for the images shown in (b) and (c).

5. Conclusion

In conclusion we have shown a technique to image sub-diffraction-limited periodic and non-periodic features in the far-field. This technique is reliant on fluorescent excitation of SPPs and in-plane scattering of SPPs from surface features, rather than traditional perpendicular diffraction through surface features, or existing far-field superlenses which require specific periodic patterning of the metal lens layer. Furthermore, we have shown the unprecedented capability of this technique to image features as small as ~λ/7, appearing to be largely limited by sample fabrication and camera resolution.

Acknowledgments

This work was partially supported by the NSF CAREER Award (ECCS-0954490).

#171631 - $15.00 USD Received 3 Jul 2012; revised 1 Aug 2012; accepted 22 Aug 2012; published 28 Aug 2012